ACS Photonics

Article

pubs.acs.org/journal/apchd5

Tunable Lyotropic Photonic Liquid Crystal Based on Graphene Oxide

Peng Li,[†] Minhao Wong,[†] Xi Zhang,[‡] Haiqing Yao,[†] Ryohei Ishige,[§] Atsushi Takahara,[§] Masahiro Miyamoto,[⊥] Riichi Nishimura,[⊥] and Hung-Jue Sue*[,†]

[†]Polymer Technology Center, Department of Mechanical Engineering, Texas A&M University, College Station, Texas 77843, United States

[‡]Kaneka Americas Holding Inc., Pasadena, Texas 77507, United States

[§]Department of Applied Molecular Chemistry, Institute for Materials Chemistry and Engineering, Kyushu University, , Fukuoka 819-0395, Japan

[⊥]Corporate R&D Division, Kaneka Corporation, Osaka 530-8288, Japan

Supporting Information

ABSTRACT: A direct colloidal self-assembly approach was utilized to prepare photonic crystals based on exfoliated graphene oxide (GO) in aqueous solution. The GO sheets form ordered photonic structure spontaneously without the need for multiple processing steps. The wavelength of light reflected by the GO photonic crystal dispersion can be controlled over the entire visible light spectrum simply by varying the GO concentration. The aspect ratio of the GO sheets and mediation of the intersheet forces are found to be the key factors influencing the stability of photonic crystal formation. The usefulness and limitations of the GO photonic crystals prepared in this study are discussed.

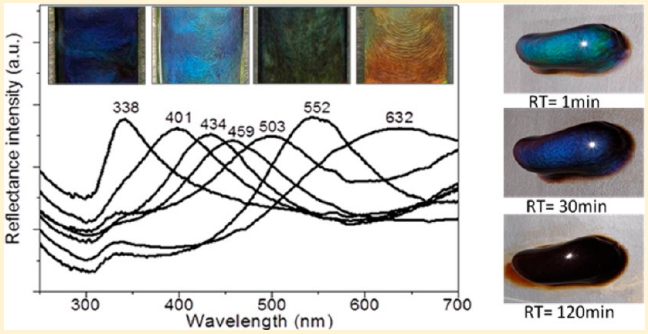

KEYWORDS: *graphene oxide, photonic crystal, structural coloration, aspect ratio, colloidal interaction*

An intriguing phenomenon in nature is structural coloration, which is commonly developed in biological communication, mimicry, and mate selection.[1−3] An exemplary example of structural coloration can be observed in the fruit *Pollia condensata*, which exhibits a brilliant iridescent color caused by Bragg reflection of periodically stacked multilayers of cellulose microfibrils.[4] In the realm of chemistry, structural coloration in solutions of surfactant and inorganic nanoplatelets has been demonstrated, which is caused by the formation of long-range ordered mesophases.[5,6] Essentially, when periodic photonic structures with interlamellar spacing on the order of the wavelength of visible light are formed, structural coloration or iridescence occurs, i.e., Bragg reflection in the visible wavelengths. These photonic materials have attracted significant attention in recent years due to their application in controlling propagation of light at a different range of frequencies.[7,8]

Self-assembly of photonic structure based on colloidal two-dimensional (2D) inorganic nanoplatelets has been extensively investigated.[6,9,10] Repulsion (Coulombic or steric) and attraction (van der Waals, Coulombic, or depletion interaction) are the major tools applied to govern the colloidal self-organization process.[11,12] Gabriel et al.[10] studied inorganic $H_3Sb_3P_2O_{14}$ nanoplatelet dispersion, which forms a gel-like lamellar phase in aqueous solution. Iridescence was observed as water swells the $H_3Sb_3P_2O_{14}$ gel to increase interlamellar spacing to an appropriate distance. It was also reported[6] that sterically stabilized gibbsite nanoplatelet suspensions exhibited strong Bragg reflection in the visible light range due to the formation of long-range smectic liquid crystal phases. These oriented colloidal platelets can be used as templates for generation of ordered solid structures with unique photonic properties.[9] Moreover, if functional 2D platelets with a unique set of properties are utilized, then it is possible to design materials with advanced properties tailored across different functionalities and multiple length scales.

Compared to inorganic 2D nanoplatelets, graphene and its derivatives have attracted unusual attention due to its unique mechanical, thermal, optical, and electronic properties.[13−16] Chemically derived graphene oxide (GO) has traditionally served as a precursor for synthesizing graphene on a large scale. Because of its easy processability, water solubility, heterogeneous electronic structure, and accessible oxygen-containing functional groups, GO shows great potential in various nanotechnology applications, including solar cells, cellular imaging, chemical and biological sensors, and advanced optoelectronics devices.[17−20] Compared with graphene, GO is fluorescent over a broad range of wavelengths due to the recombination of electron−hole pairs in localized electronic states.[21,22] The embedded oxygen-containing functional groups

Received: October 27, 2013
Published: December 30, 2013

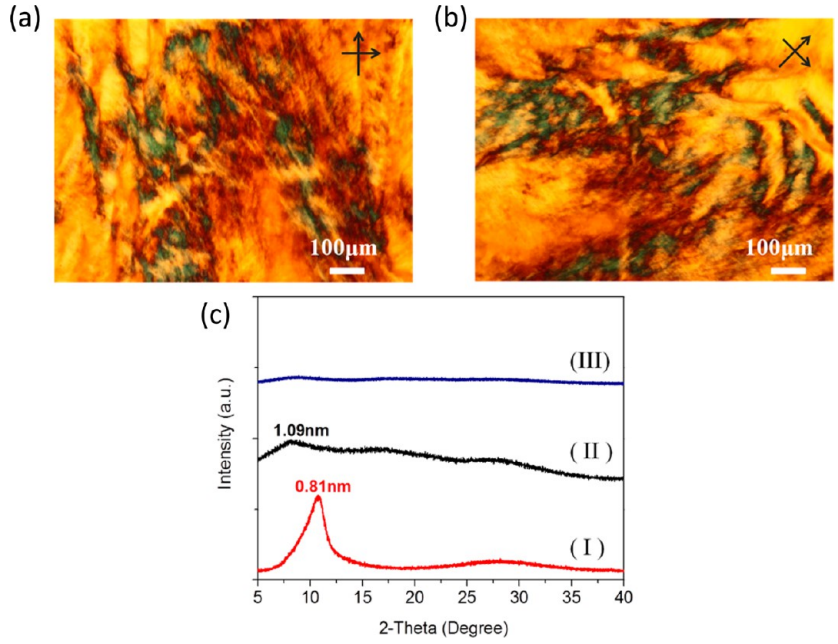

Figure 1. Cross-polarized light optical micrographs of the GO-L aqueous dispersion (0.4 vol %) with a sample rotation of (a) 0° and (b) 45°. (c) XRD results of the GO aqueous dispersions. Note that (I) is as-prepared GO, (II) is GO after stirring, and (III) is GO after stirring and removal of unexfoliated particles.

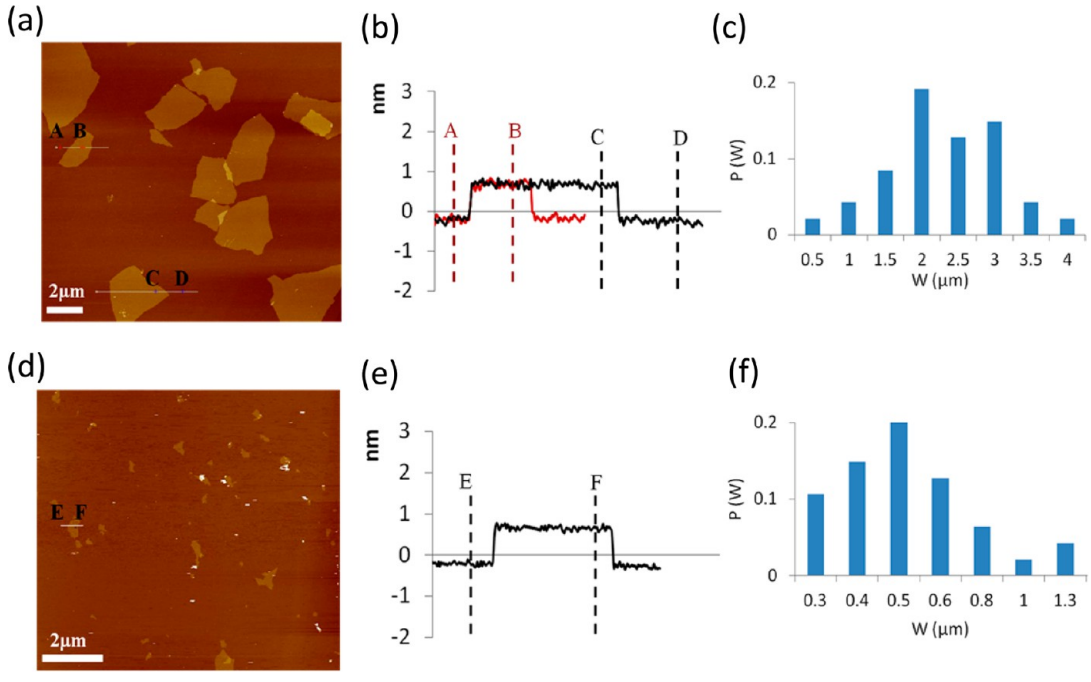

Figure 2. (a, d) Tapping-mode AFM images, (b, e) height profiles, and (c, f) width distributions of GO. (a)−(c) are GO-L, while (d)−(f) are GO-S.

also allow GO to interact with various organic and inorganic species for preparation of advanced functional hybrids.[23,24] Furthermore, chemical reduction of GO through the removal of oxygen species and/or rearrangement of carbon atoms can achieve the recovery of sp^2 network structure, which provides a pathway for tailoring its optoelectronic properties.[25] However, exfoliated GO usually exhibits irregular size, shape, and wrinkled surface morphology. Therefore, it is extraordinarily challenging to manipulate colloidal GO to form a long-range ordered structure without using complex chemical treatment or confinement. Recently, Gao et al.[26] reported liquid crystal behavior based on GO aqueous dispersion, which shows multiple colors under polarized light conditions. However the GO liquid crystals do not generate any structural color under natural light. To our knowledge, there is no known literature reporting GO-based photonic structure through direct colloidal self-organization exhibiting tunable structural color over the entire visible light spectrum to date.

Here, we report the preparation of GO photonic crystal dispersion in an aqueous solution via a simple self-assembly approach. The light reflection from the GO photonic dispersion can be tuned to cover the entire visible spectrum simply by

dx.doi.org/10.1021/ph400093c | ACS Photonics 2014, 1, 79−86

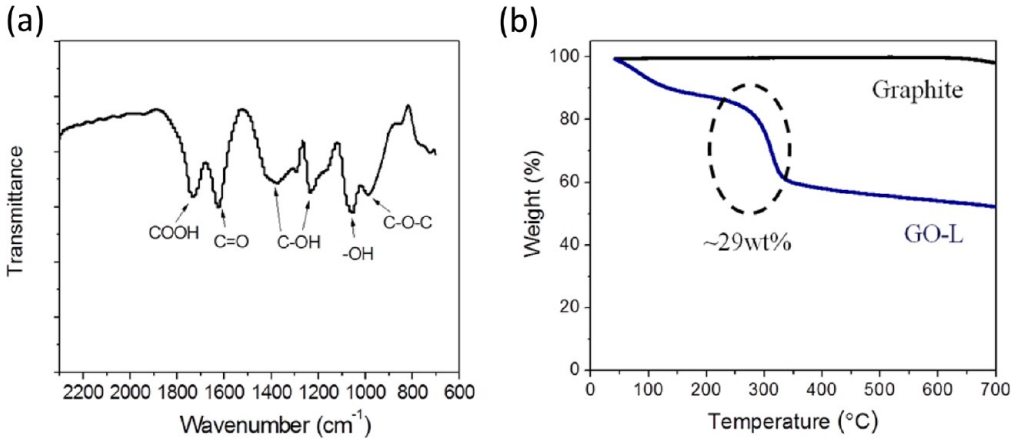

Figure 3. (a) FTIR-ATR spectrum of GO-L. (b) TGA spectra of graphite and GO-L.

varying the GO concentration. Various factors that affect the formation of GO photonic structure are discussed. The present findings show feasibility of development of novel graphene-based materials for potential applications in sensors, tunable reflective filters, and many other optoelectronic devices.[27,28]

RESULTS AND DISCUSSION

Preparation and Exfoliation of GO. In this work, a facile amphiphilic self-assembly approach to fabricate GO-based photonic crystals with obvious structural coloration under white light is reported. GO can be considered a negatively charged amphiphilic molecule due to its combination of hydrophilic oxygen-containing functional groups and a hydrophobic basal plane.[30,31] The successful preparation of the unique GO photonic structure does not require complex procedures. Rather, it is achieved by tailoring GO synthesis and manipulating the colloidal interaction during the self-assembly process.

The GO utilized in this study was synthesized by a modified Hummers method,[29] then exfoliated in water with the aid of mechanical stirring. As shown in Figure 1c, the X-ray diffraction (XRD) pattern of as-prepared GO dispersion before exfoliation exhibits a diffraction peak at $2\theta = 10.8°$, which corresponds to an interlayer spacing of 0.81 nm. After mechanical stirring, this diffraction peak disappears, suggesting that most of the GO sheets have been exfoliated or intercalated. However, a small peak at $2\theta = 8.1°$ was still observed, which corresponds to an interlayer d-spacing of 1.09 nm. This indicates the presence of unexfoliated GO residue in the dispersion. The increased d-spacing from 0.81 to 1.09 nm is possibly due to the formation of hydrogen-bonded networks, which involve functional groups on the GO surface and water molecules within the interlayer cavities.[32] A limited amount of unexfoliated GO residue (~15 wt %) was then carefully removed by centrifugation. After that, no observable XRD diffraction peaks could be detected (Figure 1c), indicating the presence of a well-exfoliated GO aqueous dispersion. The GO suspension was further characterized using atomic force microscopy (AFM) to confirm its exfoliation state. As shown in Figure 2, the GO sheets are indeed exfoliated with a thickness of about 0.9 nm. This thickness is larger than that of an ideal graphene sheet due to the presence of oxygen-containing functional groups on the GO basal plane.[24] Finally, the presence of lyotropic mesomorphism of GO-L in aqueous solution was demonstrated through cross-polarized light observation (Figure 1a,b).

Factors Influencing the Formation of GO Photonic Crystals. An obvious factor that influences the formation of GO photonic structure is the aspect ratio (α), which is defined as the GO sheet diameter divided by its thickness. It is intuitively clear that the aspect ratio of GO sheets can greatly affect their properties.[33,3435] However, upon oxidation and sonication, the GO sheets are usually cut into small pieces and exhibit a wide size distribution.[36] To study the effect of GO size on the formation of its photonic structure, both GO-L and GO-S were prepared using a pH-assisted selective sedimentation technique proposed by Shi et al.[36] As shown in Figure 2, the AFM results indicate that the average sizes of GO-L and GO-S are about 2.4 μm and 550 nm, respectively. The relative sizes between GO-L and GO-S were assessed by dynamic light scattering (DLS) via three different measurement modes (Supplemental Figure S1). Interestingly, the GO-L aqueous dispersion at certain concentrations exhibits structural color under natural light. In contrast, the GO-S dispersion does not show a similar iridescent color at any concentration. Moreover, it is commonly known that upon moderate sonication, the size of GO sheets is usually decreased.[36] When the original GO-L aqueous dispersion that shows structural color was sonicated for 2 h (Branson 2510), its iridescent color would disappear. This confirms that the GO aspect ratio plays an important role in its photonic response to natural light.

The process of amphiphilic GO self-assembly is an interplay of enthalpy change (ΔH) and entropy change (ΔS) as shown in eq 1:

$$\Delta G_{\text{self-assembly}} = \Delta H_{\text{self-assembly}} - T\Delta S_{\text{self-assembly}} \quad (1)$$

Studies[37,38] into the thermodynamic driving force for amphiphilic self-assembly into liquid crystal phases indicate that the entropic contribution plays a dominant role, while the enthalpy change is unfavorable in most cases. Onsager's theory[39] predicts that high aspect ratio particles can form liquid crystal phases above a critical volume fraction due to a net gain in entropy as the loss of orientational entropy is compensated by an increased translational entropy. Specifically, higher aspect ratio particles favor the formation of long-range liquid crystalline phases. Another possible reason for the GO aspect ratio effect could be the structural corrugation of GO sheets in solvent as the restoring force originated from bending the sheets is much weaker than that along the sheet. It was found that the degree of GO corrugated morphology in solvent could be further enhanced if its aspect ratio is increased. This

dx.doi.org/10.1021/ph400093c | ACS Photonics 2014, 1, 79−86

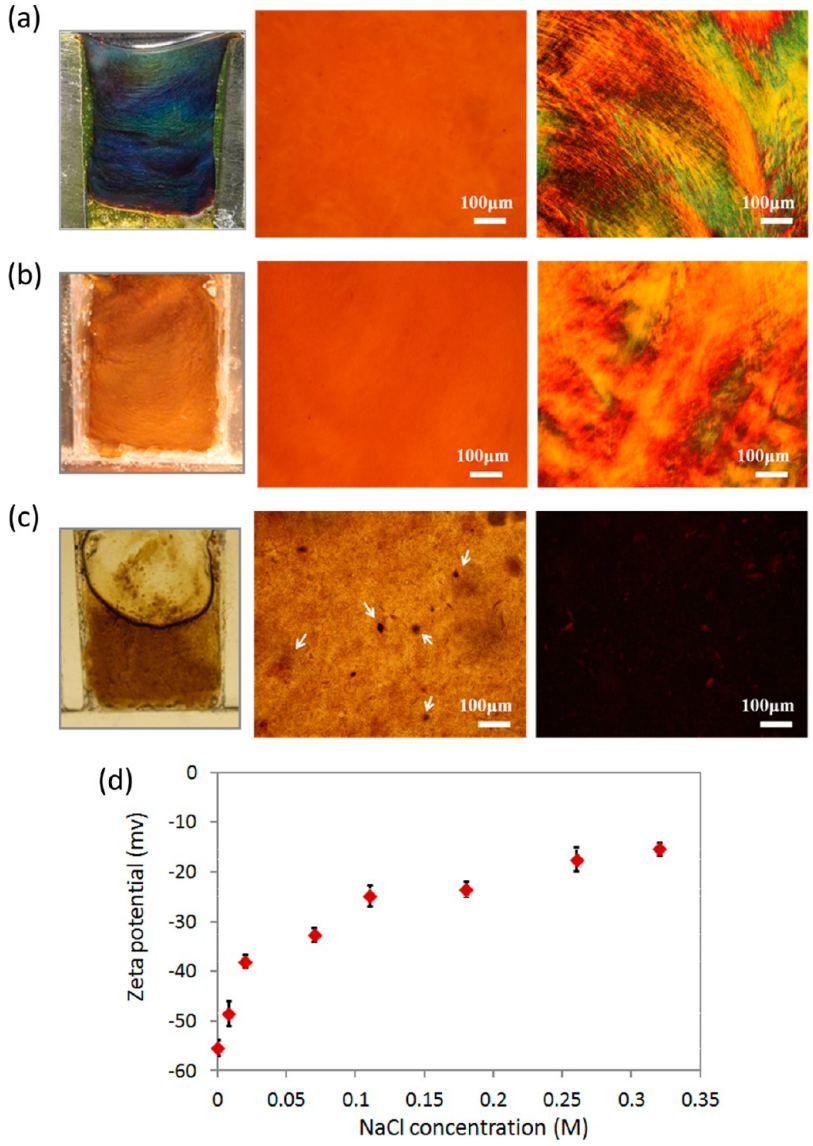

Figure 4. Optical images of a GO-L aqueous dispersion at NaCl concentrations of (a) 1.2×10^{-5} M, (b) 0.008 M, and (c) 0.3 M (left: photographical images; middle: OM images; right: cross-polarized OM images). The white arrows in (c) indicate GO-L aggregates. (d) Zeta potential of a GO-L aqueous dispersion as a function of NaCl concentration.

corrugated configuration will significantly affect both the intra- and intermolecular interactions of GO in suspension.[40−43]

To achieve iridescence in an aqueous dispersion, well-exfoliated GO sheets with strong long-range electrostatic repulsion are required. Formation of photonic structures out of colloidal particles typically requires a delicate balance of long-range repulsive forces, such as electrostatic forces, and short-range attractive forces, such as van der Waals forces and $\pi-\pi$ interactions. If the long-range repulsive forces are not strong enough to overcome the short-range attractive forces, aggregation of colloidal particles or formation of a lyotropic liquid crystal with small periodicity will inevitably occur. In the GO aqueous dispersion, long-range repulsive interactions are offered by the electrical double layers formed by the ionized oxygen functional groups.[44] Although GO sheets still contain a considerable portion of hydrophobic domains, attractive $\pi-\pi$ interactions and van der Waals forces can be effectively overcome by adjusting the long-range electrostatic repulsive forces.[44,45]

The chemical composition of GO plays an important role in tailoring the electrostatic interaction in an aqueous dispersion. The increase of surface charge density will lead to an increase in the strength of the electrostatic repulsion against the attractive forces. The ratio of the aromatic and oxygenated domains can be easily tuned by the level of graphite oxidation.[46,47] The Fourier transform infrared spectroscopy under attenuated total reflectance mode (FTIR-ATR) results of the GO-L (Figure 3a) indicate that oxidized species (hydroxyl, epoxy, and carboxyl groups) exist on the GO-L surfaces. As shown in Figure 3b, thermogravimetric analysis (TGA) in nitrogen was used to probe the oxygen functional group density on the GO-L surface. A mass loss of ∼29 wt % is found at around 250 °C and is attributed to the decomposition of labile oxygen-containing species. Below 160 °C, a mass loss of ∼17 wt % is observed, corresponding to desorption of physically absorbed water. The X-ray photoelectron spectroscopy (XPS) result of GO-L (Supplemental Figure S2) shows that an atomic ratio of C/O is about 1.9. This suggests that the GO-L has a relatively higher

dx.doi.org/10.1021/ph400093c | ACS Photonics 2014, 1, 79−86

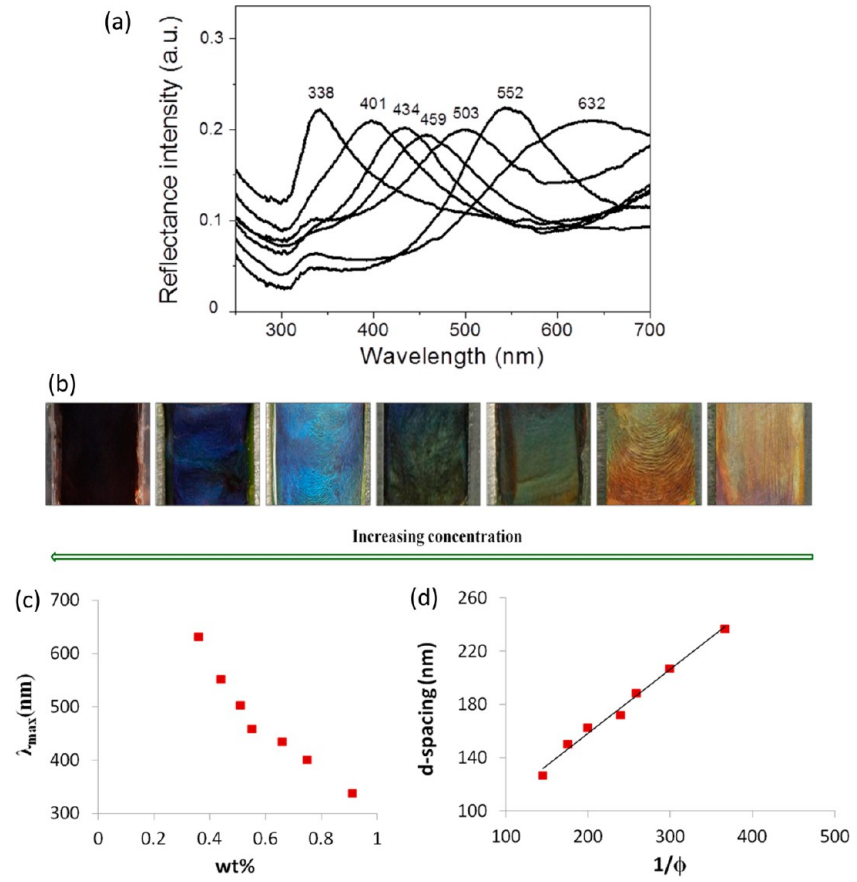

Figure 5. (a) Optical reflectance spectra and (b) visual images of GO-L dispersions of different structural colors. From left to right the weight fraction of GO-L is 0.91, 0.75, 0.67, 0.55, 0.51, 0.44, and 0.36 wt %, respectively. (c) Peak positions (λ_{max}) of reflectance spectra versus GO-L wt %, demonstrating the dependence of iridescent color on GO-L concentration. (d) *d*-Spacing exhibits a linear dependence on the inverse volume fraction ($1/\phi$). *d*-Spacing was calculated from $d = \lambda_{max}/2\eta$.

density of oxygen functional groups compared to that of the GO reported in the literature.[33,34,48] In contrast, we also prepared GO containing a lower density of oxygen functional groups by simply reducing the graphite oxidation time. In this case, no iridescent color was observed.

The colloidal interaction between GO sheets can be significantly influenced by the ionic strength, because the Debye screening length (κ^{-1}) can be effectively increased by reducing the concentration of free ions surrounding GO sheets. It was reported that the electrostatic repulsion of the GO liquid crystal in water will decrease as the salt concentration increases.[20] As a result, more water is expelled from the GO interlamellar space with an accompanying reduction in *d*-spacing. Thus, ionic impurities in the GO dispersions should be sufficiently removed, as it is a crucial factor influencing the formation of GO photonic structure. In our experiment, inductively coupled plasma mass spectrometer (ICP-MS) testing shows that the concentration of the [Na^+] in the GO-L photonic dispersion after sufficient washing is about 1.2×10^{-5} M. As shown in Figure 4a, the original GO-L photonic liquid with a pH value of 4.5 shows a blue color if no NaCl is added. However, the structural coloration disappears when [Na^+] is more than 0.008 M (Figure 4b). This is likely due to the screening of electrostatic interactions and the consequent reduction of interlayer spacing at high ionic strength. Furthermore, the optical micrographs (OM) results (Figure 4b) indicate that the GO-L dispersion at [Na^+] ≈ 0.008 M is stable without detectable precipitation, and its dispersion still exhibits birefringent behavior. As [Na^+] rises to 0.3 M, flocculated GO-L aggregates appear (Figure 4c), implying that an increasing salt content significantly weakens the repulsive force, thereby inducing phase segregation. Such an explanation is confirmed by tracking the zeta potentials of the GO-L dispersions with the introduction of NaCl salt (Figure 4d). The absolute value of the zeta potential decreases from 56 to 15 mV as [Na^+] increases, and precipitation occurs due to minimized repulsive forces.

Spectral and Structural Characterization of GO Photonic Crystals. A series of GO-L aqueous dispersions at different concentrations were prepared. As shown in Figure 5a, the reflectance spectra of these solutions display peak shifting from violet to red as the concentration of GO-L was gradually reduced. A slight widening of the reflection peak was observed at low GO concentration. As GO concentration increases, the GO sheets are more oriented partiality due to the "excluded volume" effects, which leads to a relatively narrower reflection peak based on Platz theory.[49] Photographic images (Figure 5b) of the solutions enclosed in the custom-made glass cells demonstrate the brilliant colors displayed by the suspended GO-L photonic crystals. GO-L concentration ranges from 0.36 to 0.91 wt %, resulting in a shift of the reflectance peak λ_{max} from 632 to 338 nm (Figure 5c). According to the equation (i.e., $d = \lambda_{max}/2\eta$) proposed by Platz et al.,[49] we estimate that in water (refractive index η = 1.333) a *d*-spacing of around 173 nm is required for iridescence to show blue color (λ_{max} = 461 nm). The evolution of interlayer spacing with respect to the

dx.doi.org/10.1021/ph400093c | ACS Photonics 2014, 1, 79−86

inverse volume fraction $(1/\phi)$ is shown in Figure 5d. In the range $0.27\% < \phi < 0.69\%$, the d-spacing exhibits a linear dependence on the inverse of GO-L volume fraction. The thickness of GO-L sheets is estimated from the slope of the trend line to be 0.48 nm, which is close to the thickness of GO-L measured by AFM, suggesting that GO-L sheets in aqueous dispersion are individually exfoliated.

As shown in Figure 6a, the GO-L aqueous dispersion in gel form inside a centrifuge tube shows brilliant structural colors

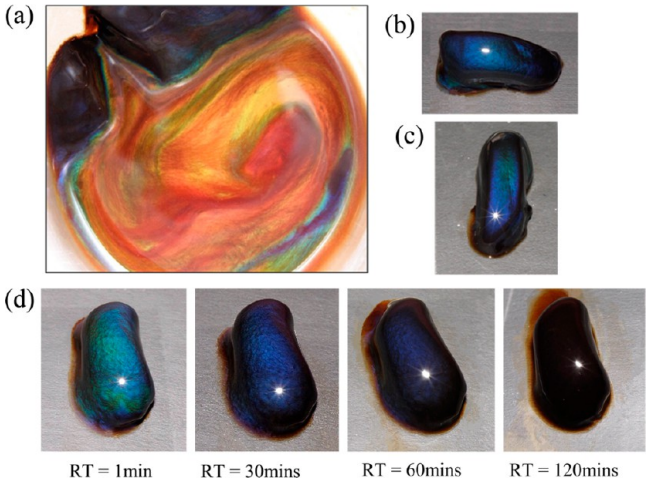

Figure 6. (a) Iridescent color of GO-L gel inside a centrifuge tube. (b and c) Color of GO-L gel on a glass slide from different viewing angles. (d) Difference in structural colors of GO-L gel with increasing resting time (RT) at room temperature. All photographs were taken under white light.

when exposed to white light, which is caused by Bragg reflection of long-range order of a GO-L lyotropic liquid crystal. Meanwhile, as the GO-L gel is transferred onto a glass slide (Figure 6b,c), its structural color can be clearly observed from different viewing angles. Moreover, the iridescent color of the GO-L gel changes from green to blue, and to black (Figure 6d), with increasing water evaporation time at room temperature. This occurs because of water evaporation from the GO-L gel that results in a decrease in interlamellar distance.

Scanning electron microscopy (SEM) and small-angle X-ray scattering (SAXS) were carried out to investigate the structure of the GO-L photonic dispersion. The local orientation of the GO-L photonic microstructure is shown in Figure 7. The GO-L photonic dispersion at different GO-L concentrations was quenched in liquid nitrogen and subsequently freeze-dried to remove water. The freeze-dried solid surfaces of the GO-L photonic dispersion exhibit ordered alignment of GO-L sheets along their planar axes as marked by white lines. Similarly, GO-L ordered texture from the cross-sectional view was also characterized (Supplemental Figure S3). SAXS 2D diffractograms and scattering intensity profiles of GO-L aqueous suspension in the concentration range from 0.36 to 1.3 wt % are shown in Supplemental Figure S4. A strong broad first peak at scattering vector $(q) = 0.078\ \mathrm{nm}^{-1}$ and a weak broad secondary peak are observed for the GO-L suspension with a concentration of 1.3 wt %, suggesting that a loosely ordered smectic GO-L structure has been formed in this concentrated suspension. In the case of a dilute GO-L suspension with concentrations from 0.36 to 0.69 wt %, no obvious first-order diffraction peaks were detected ($0.063\ \mathrm{nm}^{-1} < q < 3.9\ \mathrm{nm}^{-1}$).

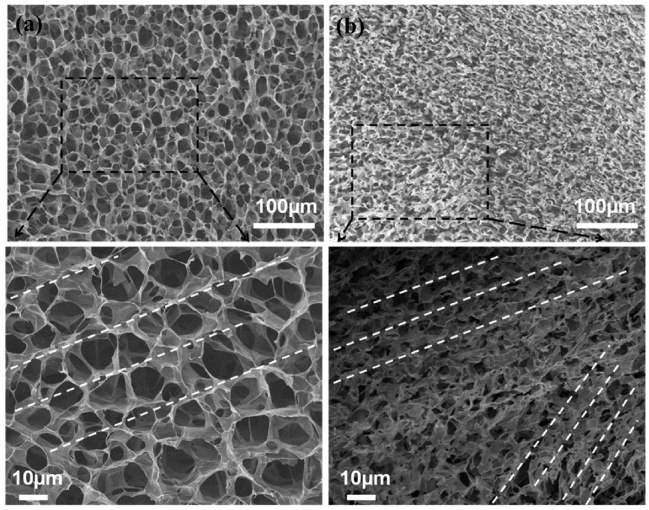

Figure 7. SEM images of the surface of freeze-dried GO-L photonic structures at GO-L concentrations of (a) 0.36 wt % and (b) 0.91 wt %, respectively. The dashed white lines indicate the alignment direction of the GO-L sheets.

This is likely due to either the low level of lamellar positional order or the interlamellar spacing is too large to be detected.

Colloidal self-assembly is an efficient and inexpensive approach for the fabrication of photonic crystal structures, especially for applications where presence of small defects can be tolerated. The straightforward control of the GO photonic structure by changing GO concentration makes it attractive for many potential applications, such as tunable reflective filters and sensors. The versatility in decoration of chemical functionality on GO surfaces along with its tunable energy band gap offers opportunities for new exciting optoelectronic applications. For instance, magnetically or electrically responsive photonic materials based on GO hybrids will likely exhibit a controllable and reversible photonic response along the direction of the external field for energy-efficient color display applications. These possibilities will soon be explored.

CONCLUSIONS

A simple, yet effective self-assembly approach has been developed to fabricate photonic structure based on large-sized amphiphilic GO in aqueous dispersion. Compared to the commonly used sophisticated lithography techniques for the preparation of photonic structures, the present method is more suitable for engineering applications because of its low cost and high yield. The color reflection by the GO photonic structure can be tuned across the entire visible spectrum through the adjustment of GO concentration. GO aspect ratio and the colloidal interactions between GO sheets are among the important factors that control the formation of GO photonic structure. The current study may significantly broaden the utilization of GO-based materials for advanced device applications.

EXPERIMENTAL METHODS

Materials. Graphite was obtained from Bay Carbon Inc. Hydrogen peroxide (H_2O_2), potassium permanganate ($KMnO_4$), barium sulfate ($BaSO_4$), and sodium nitrate ($NaNO_3$) were purchased from Aldrich and used as received.

Synthesis of GO. GO was synthesized from purified natural graphite using the modified Hummers method.[29] First, graphite

dx.doi.org/10.1021/ph400093c | ACS Photonics 2014, 1, 79−86

(0.5 g) was added into a 250 mL flask containing 50 mL of concentrated H_2SO_4 and 0.5 g of $NaNO_3$. After stirring for 20 min, the flask was immersed in an ice bath, and $KMnO_4$ (0.3 g) was slowly added during stirring. Upon oxidation for 3 h, 23 mL of deionized (DI) water was heated to 70 °C and slowly added into the mixture. After 30 min, the reaction mixture was diluted with 70 mL of 70 °C DI water, followed by the addition 10 mL of H_2O_2 to neutralize excess $KMnO_4$. Then the mixture was washed with DI water and a 5% HCl aqueous solution numerous times to remove the residual metal species.

Preparation of GO Photonic Crystal Dispersion. The GO after washing was dissolved into an aqueous suspension with a concentration of 1.5 mg/mL, followed by mechanical stirring for 2 days. Then, the GO dispersion was subjected to mild centrifugation at 3000 rpm for 7 min to remove a small amount of nonexfoliated GO particles. Subsequently, the pH value of the purified GO dispersion was adjusted to about 2.5 by using diluted HCl and stirred for 6 h. During this process, a portion of the GO became precipitated. Next, the GO sediments and residual supernatant were separated by centrifugation. The relatively small-sized residual GO in the supernatant was defined as GO-S. The sediment GO with a relatively large size was denoted as GO-L and was redispersed in an aqueous dispersion. The GO-L dispersion was further centrifuged at 12 000 rpm for 90 min. Afterward, the GO-L gelated at the bottom of centrifuge tube, which is designated as GO-L gel. The GO-L gel was then redispersed in water at different concentrations to obtain the GO-L photonic crystal dispersions.

Characterization. Scanning electron microscopy images were acquired using a JEOL JSM-7500F field emission-SEM (FE-SEM). X-ray diffraction patterns were obtained on a Bruker D8 Advanced Power X-ray diffractometer with Cu Kα incident radiation (λ = 1.5418 Å). Fourier transform infrared spectroscopy under attenuated total reflectance mode was performed using a Nicolet Avatar 360. Dynamic light scattering measurements were conducted on a Brookhaven Instruments (Holtsville, NY, USA) device. Optical micrographs were collected using an Olympus BX60 optical microscope. Inductively coupled plasma-mass spectrometry was performed using a Perkin-Elmer DRCII ICP-MS. X-ray photoelectron spectroscopy was performed with a Kratos Axis Ultra Imaging X-ray photoelectron spectrometer. Tapping-mode atomic force microscopy was carried out with a Digital Instruments Nanoscope AFM system. Thermogravimetric analysis of samples was carried out on a Q500-TGA from TA Instruments. Small-angle X-ray scattering was performed at the Japan Synchroton Radiation Research Institute (JASRI) SPring-8 facility located in Hyogo, Japan. The scattering vector is defined by $q = (4\pi/\lambda) \sin \theta$, where λ is the wavelength of the X-rays, and 2θ is the angle between the incident X-ray beam and the scattered X-rays. To demonstrate that the color of iridescence changes at various GO concentrations, reflectance spectroscopy was performed using a Shimadzu 3600 UV−vis−NIR spectrophotometer. The GO dispersions were injected into a cuvette (25.4 mm × 15.0 mm × 1.3 mm, 2.0 mm optical path length) made from two thin rectangular glass plates (Fisher-Scientific) that were double-sealed by solvent resistant epoxy (PermaPoxy 5 min) and silicone (Loctite RTV 587 Blue). White $BaSO_4$ powder was used as a standard for analyzing the reflectance of the samples.

■ ASSOCIATED CONTENT

Supporting Information

DLS of GO-L and GO-S, XPS elemental analysis of GO-L, SEM images of cross-sectional view of freeze-dried GO-L, SAXS analysis of GO-L dispersions at various GO-L concentrations. This material is available free of charge via the Internet at http://pubs.acs.org.

■ AUTHOR INFORMATION

Corresponding Author

*Fax: +1 979 845-3081. E-mail: hjsue@tamu.edu (H.-J. Sue).

Notes

The authors declare no competing financial interest.

■ ACKNOWLEDGMENTS

The authors would like to thank Rita Silbernagel for her assistance in ICP-MS experiment and Fuwu Zhang for his assistance in freeze-dried SEM work. The SAXS measurements were conducted on the BL40B2 beamline in SPring-8, Hyogo, Japan (Proposal No. 2013A1470). We would like to gratefully thank Dr. Noboru Ohta (JASRI/SPring-8) for his helpful assistance with the transmission SAXS. Financial support of this research provided by Kaneka Corporation is greatly appreciated.

■ REFERENCES

(1) Doucet, S. M.; Meadows, M. G. Iridescence: A Functional Perspective. *J. R. Soc. Interface* **2009**, *6*, 115−132.
(2) Stoddard, M. C.; Prum, R. O. How Colorful Are Birds? Evolution of the Avian Plumage Color Gamut. *Behav. Ecol.* **2011**, *22*, 1042−1052.
(3) Vukusic, P.; Sambles, J. R. Photonic Structures in Biology. *Nature* **2003**, *422*, 852−855.
(4) Vignolini, S. Pointillist Structural Color in Pollia Fruit. *Proc. Natl. Acad. Sci. U.S.A.* **2012**, *39*, 15712−15715.
(5) Hoffmann, H. Fascinating Phenomena in Surfactant Chemistry. *Adv. Mater.* **1994**, *6*, 116−129.
(6) Mourad, M. C.; Petukhov, A. V.; Vroege, G. J.; Lekkerkerker, H. N. Lyotropic Hexagonal Columnar Liquid Crystals of Large Colloidal Gibbsite Platelets. *Langmuir* **2010**, *26*, 14182−14187.
(7) Loh, K. P.; Bao, Q.; Eda, G.; Chhowalla, M. Graphene Oxide as a Chemically Tunable Platform for Optical Application. *Nat. Chem.* **2010**, *2*, 1015−1024.
(8) Soukoulis, C. M.; Wegener, M. Past Achievements and Future Challenges in the Development of Three-Dimensional Photonic Metamaterials. *Nat. Photonics* **2011**, *5*, 523−530.
(9) Mourad, M. C. D.; Groeneveld, E.; Lekkerkerkera, H. Columnar Liquid Crystals of Gibbsite Platelets as Templates for the Generation of Ordered Silica Structures. *J. Mater. Chem.* **2008**, *18*, 3004−3010.
(10) Gabriel, J.; Camerel, F.; Lemaire, B. J.; Desvaux, H.; Davidson, P.; Batail, P. Swollen Liquid-Crystalline Lamellar Phase Based on Extended Solid-like Sheets. *Nature* **2001**, *413*, 504−508.
(11) Lahiri, J.; Isaacs, L.; Grzybowski, B.; Carbeck, J. D.; Whitesides, G. M. Biospecific Binding of Carbonic Anhydrase to Mixed SAMs Presenting Benzenesulfonamide Ligands: A Model System for Studying Lateral Steric Effects. *Langmuir* **1999**, *15*, 7186−7198.
(12) Rossi, L.; Sacanna, S.; Irvine, W.; Chaikin, P. M.; Pineb, D. J.; Philipse, A. P. Cubic Crystals from Cubic Colloids. *Soft Matter* **2011**, *7*, 413−4142.
(13) Stoller, M. D.; Park, S.; Zhu, Y.; An, J.; Ruoff, R. S. Graphene-Based Ultracapacitors. *Nano Lett.* **2008**, *8*, 3498−3502.
(14) Lee, C.; Wei, X.; Kysar, J. W.; Hone, J. Measurement of the Elastic Properties and Intrinsic Strength of Monolayer Graphene. *Science* **2008**, *321*, 385−388.

(15) Bolotin, K. I.; Sikes, K. J.; Jiang, Z.; Klima, M.; Kim, P.; Stormer, H. L. Ultrahigh Electron Mobility in Suspended Graphene. *Solid State Commun.* **2008**, *146*, 351−355.
(16) Balandin, A. A.; Ghosh, S.; Bao, W.; Calizo, I.; Teweldebrhan, D.; Miao, F.; Lau, C. N. Superior Thermal Conductivity of Single-Layer Graphene. *Nano Lett.* **2008**, *8*, 902−907.
(17) Kurkina, T.; Sundaram, S.; Sundaram, R. S.; Re, F.; Masserini, M.; Kern, K.; Balasubramanian, K. Self-Assembled Electrical Biodetector Based on Reduced Graphene Oxide. *ACS Nano* **2012**, *6*, 5514−5520.
(18) Sun, X. L. Z.; Welsher, K.; Robinson, J. T.; Goodwin, A.; Zaric, S.; Dai, H. Nano-Graphene Oxide for Cellular Imaging and Drug Delivery. *Nano Res.* **2008**, *1*, 203−212.
(19) Dikin, D. A.; Stankovich, S.; Zimney, E. J.; Piner, R. D.; Dommett, G. H. B.; Evmenenko, G.; Nguyen, S. T.; Ruoff, R. S. Preparation and Characterization of Graphene Oxide Paper. *Nature* **2007**, *448*, 457−460.
(20) Xu, Z.; Gao, C. Graphene Chiral Liquid Crystals and Macroscopic Assembled Fibres. *Nat. Commun.* **2011**, *2*, 571−579.
(21) Shang, J.; Ma, L.; Li, J.; Yu, T.; Gurzadyan, G. G. The Origin of Fluorescence from Graphene Oxide. *Sci. Rep.* **2012**, *2*, 792−799.
(22) Luo, Z.; Vora, P.; Mele, E. J.; Johnson, A.; Kikkawa, J. Photoluminescence and Band Gap Modulation in Graphene Oxide. *Appl. Phys. Lett.* **2009**, *94*, 111909−111913.
(23) Eda, G.; Chhowalla, M. Chemically Derived Graphene Oxide: Towards Large-Area Thin-Film Electronics and Optoelectronics. *Adv. Mater.* **2010**, *22*, 2392−2415.
(24) Park, S.; Ruoff, R. S. Chemical Methods for the Production of Graphenes. *Nat. Nanotechnol.* **2009**, *4*, 217−224.
(25) Eda, G.; Mattevi, C.; Yamaguchi, H.; Kim, H.; Chhowalla, M. Insulator to Semi-metal Transition in Graphene Oxide. *J. Phys. Chem. C* **2009**, *113*, 15768−15771.
(26) Xu, Z.; Gao, C. Aqueous Liquid Crystals of Graphene Oxide. *ACS Nano* **2011**, *4*, 2908−2915.
(27) Shopsowitz, K.; Qi, H.; Hamad, W.; MacLachlan, M. Free-standing Mesoporous Silica Films with Tunable Chiral Nematic Structures. *Nature* **2010**, *468*, 422−425.
(28) Castles, F.; Day, F. V. Blue-Phase Templated Fabrication of Three-Dimensional Nanostructures for Photonic Applications. *Nat. Mater.* **2012**, *11*, 599−603.
(29) Hummers, W. S.; Offeman, R. E. Preparation of Graphitic Oxide. *J. Am. Chem. Soc.* **1958**, *80*, 1339−1339.
(30) Cote, L.; Kim, J.; Tung, V.; Luo, J.; Kim, F.; Huang, J. Graphene Oxide As Surfactant Sheets. *Pure Appl. Chem.* **2011**, *83*, 95−110.
(31) Kim, J.; Cote, L.; Kim, F.; Yuan, W.; Shull, K.; Huang, J. Graphene Oxide Sheets at Interfaces. *J. Am. Chem. Soc.* **2010**, *132*, 8180−8186.
(32) Medhekar, N. V.; Ramasubramaniam, A.; Ruoff, R. S.; Shenov, V. B. Hydrogen Bond Networks in Graphene Oxide Composite Paper: Structure and Mechanical Properties. *ACS Nano* **2010**, *4*, 2300−2306.
(33) Stankovich, S.; Piner, R. D.; Chen, X.; Wu, N.; Nguyen, S.; Ruoff, R. S. Stable Aqueous Dispersions of Graphitic Nanoplatelets via the Reduction of Exfoliated Graphite Oxide in the Presence of Poly(sodium 4-styrenesulfonate). *J. Mater. Chem.* **2006**, *16*, 155−158.
(34) Zhang, W.; He, W.; Jing, X. Preparation of a Stable Graphene Dispersion with High Concentration by Ultrasound. *J. Phys. Chem. B* **2010**, *114*, 10368−10373.
(35) Kim, J. E.; Han, T.; Lee, S.; Kim, S. Graphene Oxide Liquid Crystals. *Angew. Chem., Int. Ed.* **2011**, *50*, 3043−3047.
(36) Wang, X.; Bai, H.; Shi, G. Size Fractionation of Graphene Oxide Sheets by pH-Assisted Selective Sedimentation. *J. Am. Chem. Soc.* **2011**, *133*, 6338−6342.
(37) Ray, A. Solvophobic Interactions and Micelle Formation in Structure Forming Nonaqueous Solvents. *Nature* **1971**, *231*, 313−315.
(38) Greaves, T. Ionic Liquids as Amphiphile Self-Assembly Media. *Chem. Soc. Rev.* **2008**, *37*, 1709−1726.
(39) Onsager, L. The Effects of Shape on the Interaction of Colloidal Particles. *Ann. N.Y. Acad. Sci.* **1949**, *51*, 627−659.
(40) Morozov, S. V.; Novoselov, K. S.; Katsnelson, M. I.; Schedin, F.; Ponomarenko, L. A.; Jiang, D.; Geim, A. K. Strong Suppression of Weak Localization in Graphene. *Phys. Rev. Lett.* **2006**, *97*, 16801−16805.
(41) Luo, J.; Jang, H.; Huang, J. Effect of Sheet Morphology on the Scalability of Graphene-Based Ultracapacitors. *ACS Nano* **2013**, *7*, 1464−1471.
(42) Luo, J.; Jang, H.; Sun, T.; Xiao, L.; He, Z.; Katsoulidis, A.; Kanatzidis, M.; Huang, J. Compression and Aggregation Resistant Particles of Crumpled Soft Sheets. *ACS Nano* **2011**, *5*, 8943−8949.
(43) Luo, J.; Kim, J.; Huang, J. Material Processing of Chemically Modified Graphene: Some Challenges and Solutions. *Acc. Chem. Res.* **2013**, *46*, 2225−2234.
(44) Cheng, C.; Li, D. Solvated Graphenes: An Emerging Class of Functional Soft Materials. *Adv. Mater.* **2012**, *25*, 13−30.
(45) Paredes, J. I.; Villar-Rodil, S.; Martínez-Alonso, A.; Tascón, J. M. Graphene Oxide Dispersions in Organic Solvents. *Langmuir* **2008**, *24*, 10560−10564.
(46) Larciprete, R.; Fabris, S.; Sun, T.; Lacovig, P.; Baraldi, A.; Lizzit, S. Dual Path Mechanism in the Thermal Reduction of Graphene Oxide. *J. Am. Chem. Soc.* **2011**, *133*, 17315−17321.
(47) Ganguly, A.; Sharma, S.; Papakonstantinou, P.; Hamilton, J. Probing the Thermal Deoxygenation of Graphene Oxide Using High-Resolution in Situ X-ray-Based Spectroscopies. *J. Phys. Chem. C* **2011**, *115*, 17009−17019.
(48) Park, S.; Ruoff, R. S. Hydrazine-Reduction of Graphite- and Graphene Oxide. *Carbon* **2011**, *49*, 3019−3023.
(49) Platz, G.; Thunig, C.; Hoffmann, H. Iridescent Phases in Aminoxide Surfactant Solutions. *Prog. Colloid Polym. Sci.* **1990**, *83*, 167−175.